Acid Autocatalysis and Front Propagation in Water−in−Oil Microemulsions

ARTICLE *in* THE JOURNAL OF PHYSICAL CHEMISTRY C · JANUARY 2008

Impact Factor: 4.77 · DOI: 10.1021/jp076238s

4 AUTHORS, INCLUDING:

Stephen K. Scott
University of Leeds
204 PUBLICATIONS **3,602** CITATIONS
SEE PROFILE

Annette F Taylor
The University of Sheffield
51 PUBLICATIONS **597** CITATIONS
SEE PROFILE

Acid Autocatalysis and Front Propagation in Water-in-Oil Microemulsions

Rachel E. McIlwaine, Hayley Fenton, Stephen K. Scott, and Annette F. Taylor*

School of Chemistry, University of Leeds, LS2 9JT, U.K.

Received: August 3, 2007; In Final Form: November 28, 2007

Experimental results are presented of an acid autocatalytic reaction (the bromate-sulfite clock reaction) performed in water-in-oil (w/o) microemulsions with neutral (Triton X-100, TX) or cationic (CTAB) surfactants. The characteristics of the pH-sensitive reaction in the stirred system are found to depend on the molar ratio of water to surfactant (ω_0) and the nature of the surfactant. The well-stirred reaction (clock) time is faster in the TX w/o microemulsion and slower in the CTAB w/o microemulsion compared to the aqueous phase clock. The pH change is reduced in the TX system and the initial and final pH are shifted to higher values in the CTAB system. The unstirred water-in-oil microemulsions support propagating acid reaction fronts with speeds up to a factor of 10 lower than the aqueous phase fronts. The results are explained through consideration of the effect of the confinement of water in the nanosized droplets on rates and equilibria and assuming front propagation is driven by the diffusion of hydrated reverse micelles.

Introduction

Microemulsions are optically transparent, isotropic mixtures of oil, water, and surfactant. For certain compositions, the mixture self-organizes to form reverse micelles consisting of droplets of water of typical diameter 1−100 nm that are stabilized by a layer of surfactant molecules from the continuous oil phase. Hydrated reverse micelles are generally referred to as water-in-oil (w/o) microemulsions.[1] The components for a chemical reaction can be incorporated into two separate w/o microemulsions; reaction occurs upon mixing. Such media have been exploited for the synthesis of inorganic nanoparticles[2] and inducing rate enhancement or regiospecificity in organic reactions[3,4] through favorable partitioning of reactants between the aqueous and oil pseudophases.

As well as being of commercial interest, reactions in hydrated reverse micelles are often used as simplified models of reactions in biological cells.[5,6] Of particular current interest is the influence of the confinement of the water molecules in nanosized droplets on reaction dynamics and kinetics.[7] Water associated with the polar headgroups of the surfactant at the interface of the droplet forms a hydration layer containing "bound" water molecules.[8] With increasing water content, a pool forms in the micellar core with characteristics that more resemble those of bulk "free" water molecules. The size of the water pool is determined by the water/ surfactant ratio, ω_0. In general, an increase in ω_0 is correlated with an increase in the diameter of the droplets.[9]

However, even in droplets containing thousands of water molecules the disruption of the hydrogen bond network and associated changes in the water properties, such as a reduction in micropolarity and increased microviscosity, have a profound affect on the reaction rates.[10] The destabilization of charged transition states by less polar water results in a retardation of reactions involving the formation of charged species.[10,11] The increase in microviscosity reduces the rates of diffusion-controlled reactions in the droplets.[12] Reaction rates also depend on the nature of surfactant used as charged species migrate to, or are repulsed from, ionic headgroups and hence experience a different water environment depending on their location.[13] Clearly, interpretation of kinetics in these nanoreactors is complex.

Nonlinear, autocatalytic, reactions are particularly sensitive to their environment and oscillatory reactions are capable of displaying complex patterns in nanostructured media.[14,15] To date, nonlinear pH reactions have not been performed in water-in-oil microemulsions. In stirred batch reactors, acid autocatalytic reactions display an induction (clock) time during which the pH changes slowly followed by a rapid decrease in pH (autocatalytic event). When performed in a water-in-oil microemulsion, the features of the pH-sensitive reaction will depend on the properties of the aqueous pseudophase in the nanodroplets.

In unstirred reactors, autocatalytic reactions support propagating reaction fronts, driven by diffusion of the autocatalyst. Reaction fronts occur in a variety of chemical and biological systems from polymerization[16] and flame fronts,[17] to calcium fronts in cells.[18] It is therefore of interest to determine the properties of acid fronts in w/o microemulsions in which the autocatalyst is trapped in the nanodroplets. These media present interesting new possibilities in the investigation of the affect of underlying microheterogeneity on front propagation.[19,20]

In this work, we investigate the bromate-sulfite reaction in a nonionic (Triton X-100, TX) and a cationic (cetyltrimethylammonium bromide, CTAB) w/o microemulsion. This reaction is an acid autocatalytic reaction that displays both clocks and front-type behavior and has a known mechanism.[21,22] The affect of the water to surfactant molar ratio, ω_0, of the w/o microemulsion on the clock time and overall change in pH is determined. We also demonstrate that the w/o microemulsions support propagating acid fronts, the speed of which are reduced by up to a factor of 10 compared to the aqueous phase, and depend on ω_0. Novel convective instabilities are observed in the CTAB system with features that have not been observed in the aqueous phase.[23]

Experimental Methods

Both water/TX/toluene[24] and water/CTAB/1-hexanol[25] mixtures are known to form hydrated reverse micelles, or w/o

* To whom correspondence should be addressed. E-mail: A.F.Taylor@leeds.ac.uk.

10.1021/jp076238s CCC: $40.75
Published on Web 01/26/2008 PAGE EST: 6.7

microemulsions, the properties of which are characterized by two important parameters: the molar ratio of the water to surfactant, ω_0

$$\omega_0 = [H_2O]/[surf] \quad (1)$$

and the volume fraction of the reverse micelles, or droplet fraction, ϕ_d

$$\phi_d = (V_{aq} + V_{surf})/(V_{aq} + V_{surf} + V_{oil}) \quad (2)$$

where V_{aq}, V_{surf}, and V_{oil} are the volumes of the aqueous, surfactant, and oil phase, respectively. An increase in ω_0 was achieved by increasing V_{aq}, keeping V_{surf} constant and increasing V_{oil} to keep ϕ_d constant.

The w/o microemulsions were prepared by adding the aqueous phase stock solution to the nonionic surfactant Triton X-100 (Sigma) dissolved in toluene (Alfa Aesar) or the cationic surfactant cetyltrimethylammonium bromide (Sigma) dissolved in 1-hexanol (Alfa Aesar). For example, 3.05 g (V_{surf} = 3.5 mL) of CTAB was added to 8.2 mL of hexanol; 1.9 mL of aqueous solution was then supplied to the mixture, and the solution was shaken and stirred to clearness. This gave a CTAB microemulsion of ω_0 = 12.5 and ϕ_d = 0.40. A ternary phase diagram of each system was constructed from analysis of optical, conductivity, and viscosity measurements, and suitable compositions for experimentation were identified. Viscosity measurements were obtained using a Cannon-Fenske glass viscometer and conductivity was measured by using a Philips conductivity meter (cell constant = 0.78 cm^{-1}). The properties of TX varied slightly between batches as purchased, presumably due to variations in the average oxyethylene ether chain length (Figure 1a). The results reported here are for one particular batch of TX.

Aqueous stock solutions of ionic strength I = 0.3 M were prepared from analytical grade chemicals in doubly distilled deionized water (the formation of w/o microemulsions is sensitive to the ionic strength). Solution A contained sodium bromate (0.1 M, Aldrich) and sodium sulfate (0.07 M, Aldrich). Solution B consisted of a sulfite (0.06 M)/bisulfite (0.04 M) buffer prepared from sulfuric acid (1 M, Aldrich) and sodium sulfite (Aldrich) and contained bromophenol blue pH indicator (Riedel de Haen, 0.05 g/100 mL) or bromocresol purple (Sigma, 0.05 g/100 mL). This solution was continuously bubbled with nitrogen as sulfur species are prone to aerial oxidation. In this work, the initial reactant concentrations in the w/o microemulsion are recorded as the moles of species in the total volume of the aqueous pseudophase ($[X]_{0,aq}$).

The bromate-sulfite reaction was performed in the water-in-oil microemulsion by preparation of two w/o microemulsions with the same ω_0 and ϕ_d, containing the stock solutions A and B. For each batch experiment, microemulsions containing the stock solutions were freshly prepared and placed in a water bath thermostated at 23 °C. Equal amounts of the stock w/o microemulsions were then transferred into a small (20 mL) thermostated reaction vessel containing a magnetic stirrer bar to ensure complete mixing (475 rpm). The reaction rate depends on the stirring rate.[26]

A pH electrode (double junction lithium chloride/methanol, Sentek) and indicators bromophenol blue (pH transition range = 3.0−4.6) for TX experiments or bromocresol purple (pH transition range = 5.8−6.0) for CTAB experiments were used to follow the pH in time. Changes in the pH measured with the glass electrode reflect changes in the apparent pH in the droplet water pool relative to the standard pH in the aqueous phase.[27]

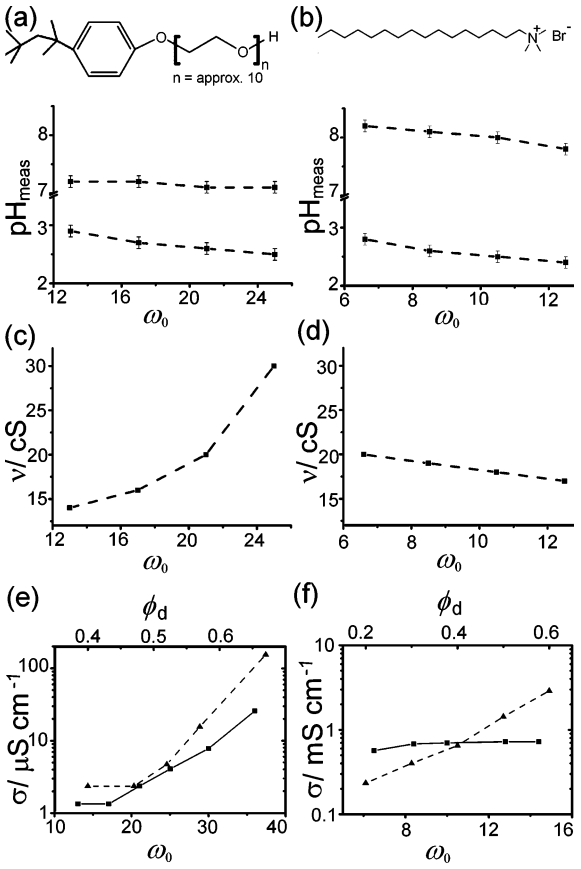

Figure 1. Measured pH of (a) TX w/o microemulsion with droplet fraction ϕ_d = 0.47 and (b) CTAB w/o microemulsion with ϕ_d = 0.40 for aqueous phase pH = 2.3 or 7.1. Kinematic viscosity of $NaBrO_3$ stock solution at 20 °C in a (c) TX w/o microemulsion with ϕ_d = 0.47 and (d) CTAB w/o microemulsion with ϕ_d = 0.40. Conductivity of $NaBrO_3$ stock solution (aqueous phase σ = 21 mS cm^{-1}) at 22 °C in a (e) TX w/o microemulsion as a function of ϕ_d (triangles, ω_0 = 19) and ω_0 (squares, ϕ_d = 0.47) and (f) CTAB w/o microemulsion as a function of ϕ_d (triangles, ω_0 = 8) and ω_0 (squares, ϕ_d = 0.4).

The reaction time measured with the electrode corresponded to the time at which a color change in the indicator was observed. The value of the final pH measured with the electrode was also reflected in the color of the indicator.

Spatial experiments were performed in glass capillary tubes of internal diameter (i.d.) = 1 or 2.6 mm filled with the reactive w/o microemulsion using a syringe. Double the amount of indicator was added to the stock solutions for spatial experiments to aid in visualization of the front. Fronts were initiated at the base of the tube by injecting a small amount of a w/o microemulsion containing the reacted (acidic) solution. Images of the propagating front were captured using a charge-coupled device camera connected to LabVIEW software and were processed using Origin.

Results

The pH of the w/o microemulsion (pH_{meas}) containing two different buffer solutions (sulfite/bisulfite with pH = 7.1 or sulfuric acid/sodium sulfate with pH = 2.3) is recorded as a function of ω_0 in Figure 1 for (a) the nonionic surfactant, TX, and (b) the cationic surfactant, CTAB. The vertical bars indicate standard deviations. The pH of the w/o microemulsions decreased with increasing ω_0 and is generally higher than that of the aqueous phase stock solution. The kinematic viscosity of the w/o microemulsions is also recorded in this figure and is greater than that of the aqueous phase (the kinematic viscosity

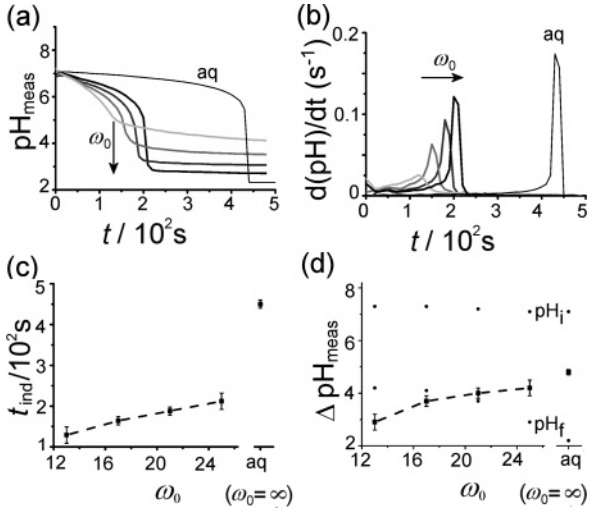

Figure 2. Bromate-sulfite clock reactions in a TX w/o microemulsion with $\phi_d = 0.47$, $[BrO_3^-]_{0,aq} = 0.05$ M, $[SO_3^{2-}]_{0,aq} = 0.03$ M, $[HSO_3^-]_{0,aq} = 0.02$ M and compared to the aqueous phase clock (aq). (a) pH time traces for $\omega_0 = 13 - 25$. (b) Rate of change of pH in time for $\omega_0 = 13-25$. (c) Variation of induction time with ω_0. (d) Variation of overall change in pH and the initial and final values of pH with ω_0.

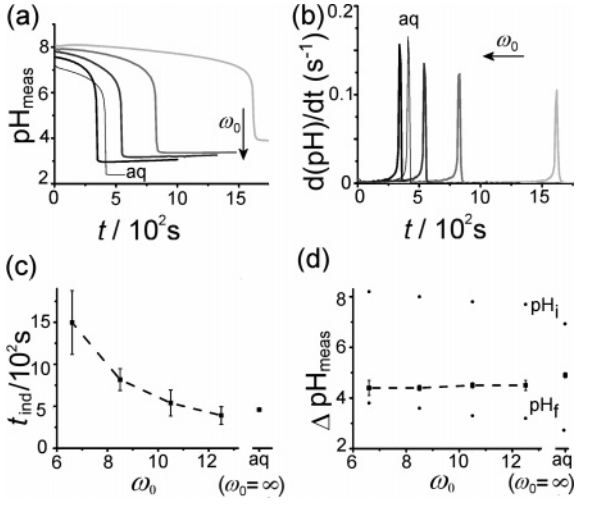

Figure 3. Bromate-sulfite clock reactions in a CTAB w/o microemulsion with $\phi_d = 0.40$, $[BrO_3^-]_{0,aq} = 0.05$ M, $[SO_3^{2-}]_{0,aq} = 0.035$ M, $[HSO_3^-]_{0,aq} = 0.015$ M and compared to the aqueous phase (aq). (a) pH time traces for $\omega_0 = 6.5 - 12.5$. (b) Rate of change of pH as a function of pH for $\omega_0 = 6.5-12.5$. (c) Variation of induction time with ω_0. (d) Variation of overall pH change and the initial and final values of pH with ω_0.

of water at 20 °C = 1 cS). The viscosity increased with increasing ω_0 in the TX system (Figure 1c) and decreased with increasing ω_0 in the CTAB system (Figure 1d).

The conductivity of the sodium bromate stock solution at 22 °C is shown as a function of both the droplet fraction ϕ_d and ω_0 in the TX w/o microemulsion (Figure 1e) and the CTAB w/o microemulsion (Figure 1f). The conductivity increases more rapidly with ϕ_d than ω_0 in the TX system. In the CTAB system, the conductivity increases steadily with ϕ_d and remains constant over the range of ω_0 used. The conductivity of toluene $<10^{-6}$ mS cm^{-1}, hexanol = 0.1 mS cm^{-1}, and the aqueous phase stock solution = 20 mS cm^{-1}.

For Triton-X w/o microemulsions, we perform kinetic experiments with $\phi_d = 0.47$ and $\omega_0 = 13-25$. Typical clock reactions in TX w/o microemulsions ($[BrO_3^-]_{0,aq} = 0.05$ M, $[SO_3^{2-}]_{0,aq} = 0.03$ M, and $[HSO_3^-]_{0,aq} = 0.02$ M) are shown in Figure 2a compared to the aqueous phase clock (aq). Clock reactions display a maximum rate at some nonzero extent of reaction. The rate of change of pH is obtained from the slope of the pH−time plot (Figure 2b) and the clock (induction) time, t_{ind}, is defined as the time to the maximum rate. The maximum rate of change of pH increased with increasing ω_0. The clock time in the w/o microemulsion is shorter than that of the aqueous phase and decreases with decreasing ω_0 (Figure 2c). The final pH is higher than the aqueous phase, and the overall pH change ($\Delta pH = pH_{initial} - pH_{final}$) decreases with decreasing ω_0 (Figure 2d).

Clock reactions in the CTAB w/o microemulsion are shown in Figure 3a with $\phi_d = 0.4$ and $\omega_0 = 6.5-12.5$. The rate of change of pH increases with increasing ω_0 (Figure 3b). For $\omega_0 = 12.5$, the clock time is shorter than that of the aqueous phase and it increases with decreasing ω_0 (Figure 3c). The clock time is less reproducible in the CTAB system than in the TX system, possibly indicating the sensitivity of this system to nonequilibrium concentration fluctuations, particularly at small ω_0.[26,28] Both the initial and final pH are higher than the aqueous phase values and increase with decreasing ω_0 (Figure 3d). The overall pH change, ΔpH, does not vary significantly with ω_0 (Figure 3d).

The bromate-sulfite reaction in a TX w/o microemulsion supports propagating fronts, converting the mixture from

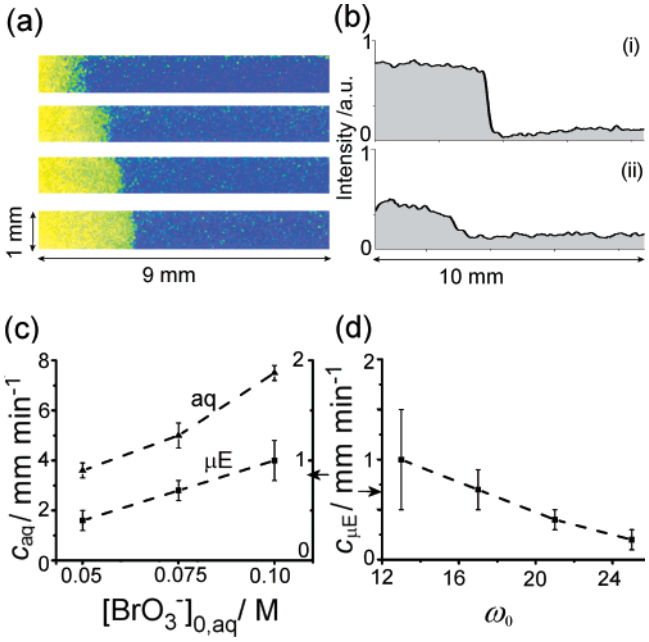

Figure 4. Acid fronts in a TX w/o microemulsion with $[BrO_3^-]_{0,aq} = 0.05$ M, $[SO_3^{2-}]_{0,aq} = 0.03$ M, $[HSO_3^-]_{0,aq} = 0.02$ M, $\phi_d = 0.47$, and $\omega_0 = 21$. (a) Color-enhanced images of the front taken at 1 min intervals. (b) Intensity profiles along the length of the tube in the (i) aqueous phase experiment and (ii) w/o microemulsion. (c) Variation of front speed, c, with initial bromate concentration in the aqueous phase (aq, left axis) and the microemulsion (μE, right axis). (d) Variation of front speed, $c_{\mu E}$, with ω_0.

reactants to products. Typical images of the fronts in horizontal glass capillary tubes of i.d. = 1 mm are shown in Figure 4a for $\omega_0 = 21$. The pH change is reduced in this system compared to the aqueous phase, and the color behind the front is green (the color is enhanced in the images shown). The position of the front is determined from intensity profiles (Figure 4b). Distance−time plots of the front were linear, and the front speed increases with increasing bromate concentration (Figure 4c). The front speed is reduced compared to the aqueous phase front speed and decreases with increasing ω_0 (Figure 4d).

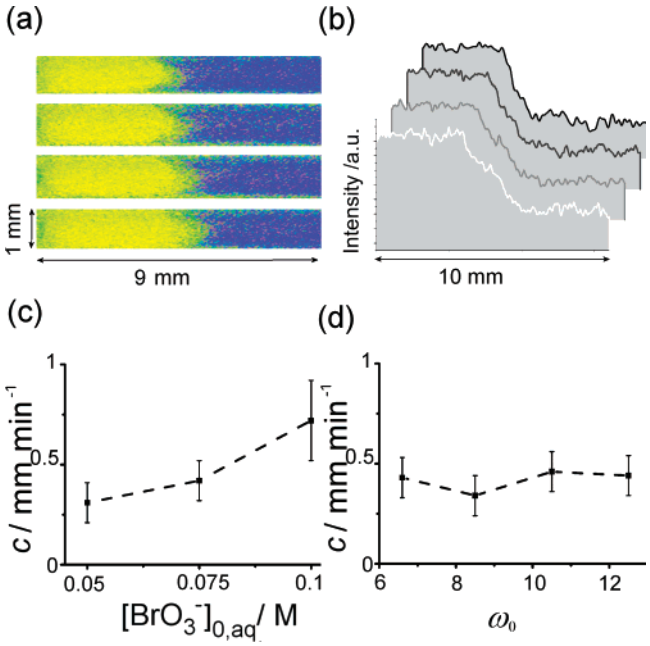

Figure 5. Acid fronts in a CTAB w/o microemulsion with $[BrO_3^-]_{0,aq}$ = 0.05 M, $[SO_3^{2-}]_{0,aq}$ = 0.03 M, $[HSO_3^-]_{0,aq}$ = 0.02 M, ϕ_d = 0.40, and ω_0 = 8.5. (a) Color-enhanced images of fronts taken at intervals of 1 min. (b) Intensity profiles along the length of the tube for the images in panel a. (c) Variation of front speed with initial bromate concentration. (d) Variation of front speed, c, with ω_0.

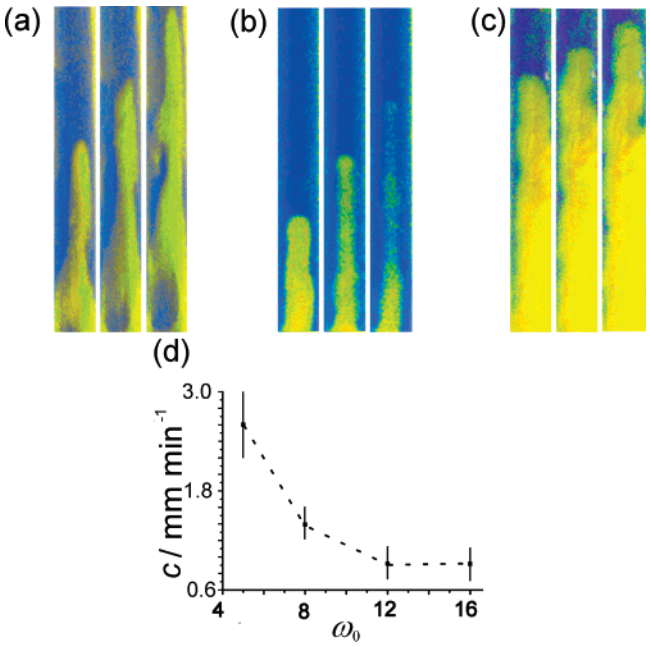

Figure 6. Temporal evolution of acid fronts in a CTAB w/o microemulsion with $[BrO_3^-]_{0,aq}$ = 0.05 M, $[SO_3^{2-}]_{0,aq}$ = 0.03 M, $[HSO_3^-]_{0,aq}$ = 0.02 M, and ϕ_d = 0.47. Color-enhanced images at 1 min intervals with a field-of-view of 2.6 × 22.1 mm and ω_0 = (a) 5, (b) 8 (10 min intervals), and (c) 16. (d) Front speed as a function of ω_0.

The CTAB system also displays reaction fronts in unstirred systems. Typical images of fronts in horizontal capillary tubes of i.d. = 1 mm are shown in Figure 5a for ω_0 = 8.5 and the corresponding intensity profiles in Figure 5b. The fronts are less sharp in the w/o microemulsion than in the aqueous phase. The front speed is reduced by a factor of 10 compared to the aqueous phase and increases with increasing bromate concentration (Figure 5c). There is no discernible trend in the front speed with ω_0 (Figure 5d). In vertical tubes of i.d. = 2.6 mm, fingers, or plumes, form at the interface between the reacted and unreacted fluid and travel through part of the tube (Figure 6). The fingers occupy a greater proportion of the tube (radially) for greater ω_0 and displayed structures that are not observed in the aqueous phase as they propagate, such as a turbulent wake (Figure 6a), an extinguishing finger (Figure 6b), or a spiral-type motion (Figure 6c). The front speed increases with decreasing ω_0 in this configuration (Figure 6d).

Discussion

The purpose of the present investigation is the examination of an acid autocatalytic reaction in a hydrated reverse micelle environment. We examined the bromate-sulfite clock reaction in a nonionic (Triton X-100) and cationic (CTAB) w/o microemulsion. In particular, we wished to determine the influence of the water-to-surfactant molar ratio, ω_0, on the characteristics of the clock reaction (clock time and overall pH change) in the well-stirred system and front propagation in the unstirred system. In general, changes in ω_0 affect reactions that occur in the water pool of the nanodroplets and changes in ϕ_d affect processes that are rate-limited by droplet collision and exchange.[29−31] The droplet fraction ϕ_d is kept constant in this work.

The Bromate-Sulfite Clock Reaction. The reaction of bromate with a sulfite-bisulfite solution is a well-known base-to-acid clock reaction in which a weak acid (bisulfite) is converted to a strong acid (hydrogen sulfate).[21,22] The reaction proceeds according to the irreversible processes 1−4 and fast equilibria 5−7:[32,33]

$$BrO_3^- + HSO_3^- \rightarrow BrO_2^- + SO_4^{2-} + H^+ \quad (1)$$

$$BrO_2^- + 2HSO_3^- \rightarrow Br^- + 2SO_4^- + 2H^+ \quad (2)$$

$$BrO_2^- + 2H_2SO_3 \rightarrow Br^- + 2SO_4^- + 4H^+ \quad (3)$$

$$BrO_3^- + H_2SO_3 \rightarrow BrO_2^- + SO_4^- + 2H^+ \quad (4)$$

$$HSO_3^- \rightleftharpoons SO_3^{2-} + H^+ \quad (5)$$

$$H_2SO_3 \rightleftharpoons HSO_3^- + H^+ \quad (6)$$

$$HSO_4^- \rightleftharpoons SO_4^{2-} + H^+ \quad (7)$$

Following Zagora et al.,[34] the mechanism is reduced to a two variable model with autocatalyst H^+ (H) and inhibitor HSO_3^- (HX)

$$\frac{dH}{dt} = -r_{HX} - 2r_{H2X} - \Delta_{HX} - \Delta_{H2X} - \Delta_{HS} \quad (8)$$

$$\frac{dHX}{dt} = r_{HX} + \Delta_{HX} - \Delta_{H2X} \quad (9)$$

where r_X are the rate contributions from irreversible reactions 1−4 and Δ_{HX} are the rate contributions from the equilibria 5−7 (see ref 34 for further details).

A typical clock simulated from the model is shown in Figure 7a. The values of the rate and equilibrium constants at the conditions in this work (23 °C, I = 0.3) are taken to be: $k_1/M^{-1}\ s^{-1}$ = 0.04, $k_2/M^{-1}\ s^{-1} = 1 \times 10^4$, $k_3/M^{-1}\ s^{-1} = 5 \times 10^{10}$, $k_4/M^{-1}\ s^{-1}$ = 18, $K_5 = 6.6 \times 10^{-8}$, $K_6 = 1.2 \times 10^{-2}$ and $K_7 = 1 \times 10^{-2}$. The induction time in this reaction can be explained by consideration of reaction 1 and the sulfite/bisulfite

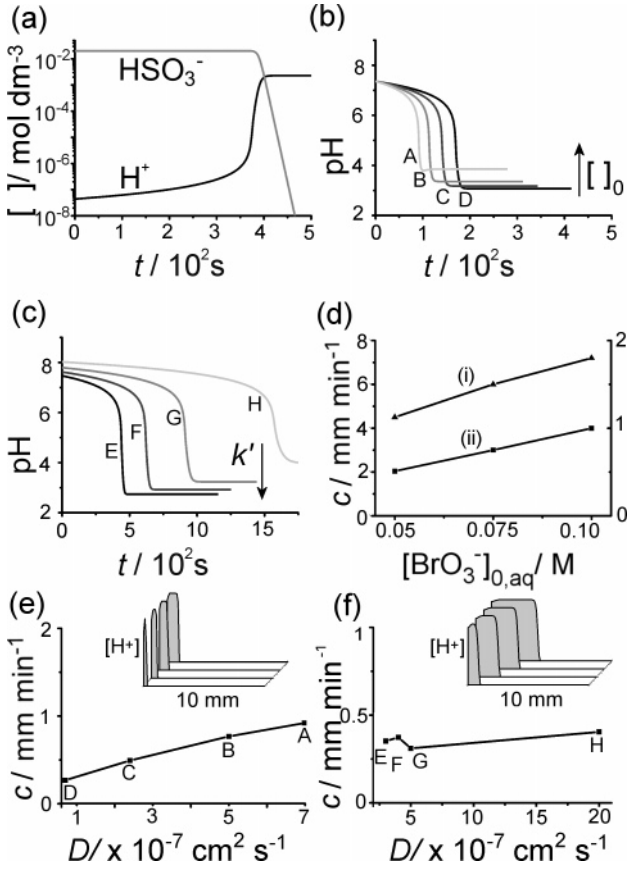

Figure 7. Simulations of the model of the bromate-sulfite clock with $[BrO_3^-]_0 = 0.05$ M, $[SO_3^{2-}]_0 = 0.03$ M, $[HSO_3^-]_0 = 0.02$ M. (a) Aqueous phase clock. (b) Clock with increasing initial concentrations ($[]_0$) and inclusion of reaction 10 (see text). (c) Clock with increasing forward rate constants (k') and inclusion of reaction 10 (see text). (d) Front speed as a function of $[BrO_3^-]_0$ with diffusion coefficient $D =$ (i) 4×10^{-5} cm^2 s^{-1} (left axis) and (ii) 2.4×10^{-7} cm^2 s^{-1} (right axis). (e) Front speed with D for clock times in panel b. Inset shows front profiles at intervals of 30 s with $D = 2 \times 10^{-7}$ cm^2 s^{-1}. (f) Front speed with D for clock times in panel c. Inset shows front profiles at intervals of 200 s with $D = 4 \times 10^{-7}$ cm^2 s^{-1}.

buffer present initially. The acid produced in reaction 1 protonates sulfite in reaction 5)thereby maintaining the $[HSO_3^-]$ until the buffer breaks down. Acid autocatalysis in this reaction can be demonstrated from consideration of reactions 4 and 6.[33,35] As the concentration of acid increases, the rate of production of H_2SO_3 increases in reaction 6, and the rate of formation of acid increases in reaction 4; thus acid catalyzes its own production.

Reaction 1 is therefore rate-determining in the consumption of SO_3^{2-}/HSO_3^- buffer and the clock time, and reaction 4 is rate-determining in the autocatalytic formation of acid. The initial pH is controlled by K_5; the final pH by K_7. Competing reactions such as the disproportionation of bromine-containing species are only important at low pH.[36]

Acid Autocatalysis in a TX w/o Microemulsion. Water added to Triton X-100 in toluene initially serves to hydrate the TX polyoxyethylene ether chains in the reverse micellar aggregates.[37] With values of ω_0 up to around 8, this bound water is effectively immobilized.[38] As the water content is increased, a water pool is formed in the core of the TX reverse micelle.[39] With $\omega_0 = 7.6-28$ in the TX system, the apparent hydrodynamic radii were found to vary from 2.7−15.0 nm and increased nonlinearly with increasing water content.[40] TX reverse micelles are most likely ellipsoidal in shape.[41]

The increase in viscosity and conductivity with ω_0 and ϕ_d (Figure 1e) may be associated with the formation of droplet clusters and percolation; Triton-X microemulsions are known to undergo a phase transition from w/o to bicontinuous to o/w upon increasing the water fraction.[42] For the values of ϕ_d (0.47) and ω_0 (13−25) chosen in this work, the water fraction varies from 14−20%, the conductivity ranges from $\sigma = 2-5\ \mu$S cm^{-1} compared to the aqueous phase conductivity of 21 mS cm^{-1}, and thus we consider the water present as individual droplets rather than an open, bicontinuous structure. We note that we cannot rule out the formation of wormlike micelles with increasing ω_0. The increase in pH in the microemulsion compared to the aqueous phase (Figure 1a) might be explained by the protonation of OH groups at the interface of the droplet.

The charged reactants in the bromate-sulfite reaction (BrO_3^- and HSO_3^-) reside preferentially in the water pool in the core of the droplet.[43] The decrease in induction time (increase in autocatalytic rate) with decreasing ω_0 may arise from an increase in the effective concentrations of the reactants in the smaller water pool of the droplets with the rest of the water residing in the interfacial TX hydration layer. The final pH of the reaction in the TX w/o microemulsion is much higher than the same microemulsion containing solution of pH = 2.3 (Figure 1). Partitioning of charged and highly polar species into the oil phase is unlikely to be significant, but loss of neutral intermediates such as H_2SO_3 into the TX hydration layer (where there is negligible BrO_3^-) needs to be considered[43]

$$H_2SO_3\,(w) \rightarrow H_2SO_3\,(i) \qquad (10)$$

where w represents the water pool and i represents the interface. Sequestration of neutral intermediates into the interfacial region will be more significant for smaller ω_0 due to the larger surface area to volume ratio of smaller droplets.

The plot in Figure 7b illustrates the effect of increasing initial concentrations and sequestration of H_2SO_3 in simulations of the model of the bromate-sulfite reaction. This plot is produced by the addition of reaction 10 with rate constant $k_{10}/s^{-1} = 1000/\omega_0^2$ and by replacing the initial concentrations by a term $[X]_0' = [X]_0 \times 50/\omega_0$.

Acid Autocatalysis in a CTAB w/o Microemulsion. Up to 7% CTAB dissolves in hexanol and forms tightly bound ion clusters.[25] Upon addition of water, the ions are hydrated and reverse micelles form of composition 1 CTAB/0.7−1 HEX/n H_2O where $n = 4-40$.[25] Hexanol therefore acts as a cosurfactant in this system. The radius of the CTAB-hydrated reverse micelles increases with increasing ω_0 (providing ω_0 is changed through increases in water fraction[44]) and depends on the concentration of CTAB. Monodisperse spherical reverse micelles of radius 34−47 nm were reported in systems with [CTAB] = 1.1 mol dm^{-3} and $\omega_0 = 4-16$.[45] The decrease in viscosity with increasing ω_0 has been observed previously and was explained by the dissolution of some of the added water in the oil phase, thereby reducing intermicellar interactions.[25]

For the value of ϕ_d (0.4) and ω_0 (6.5−12.5) chosen in this work, the water fraction increases from 9−14% and the conductivity displays no significant change ($\sigma = 0.7-0.9$ mS cm^{-1}). This is an order of magnitude higher than the hexanol conductivity (0.1 mS cm^{-1}) and an order of magnitude lower than the aqueous phase (21 mS cm^{-1}). Thus while it is unlikely there is a phase change upon increasing ω_0, elucidation of the exact structure of the w/o microemulsion containing the reactant stock solution requires further investigation. In the following discussion, we assume the solution-phase exists as closed nanodroplets.

The pH in the CTAB w/o microemulsion is shifted to higher values than the pH in the corresponding aqueous phase; the effect is more pronounced for the sulfite/bisulfite buffer solution (Figure 1). This might be explained by the migration of negatively charged species to the positively charged interface of the nanodroplets, where the water solvent mobility is the most greatly restricted.[46] The micropolarity of this environment is greatly reduced compared to the aqueous phase thus favoring ion association, that is, a decrease in K_5.

When the bromate-sulfite reaction is performed in the CTAB w/o microemulsion, the negatively charged reactants probably reside close to the droplet interface.[46] The rate of reactions that involve the formation of charged species is reduced in the less polar environment, and the effect will be largest for the smallest droplets, that is, smallest ω_0. The final pH in the CTAB w/o microemulsion is higher than the same microemulsion containing solution of pH = 2.3 (Figure 1) therefore sequestration of H_2SO_3 (reaction 10) is also possible.

The plot in Figure 7c illustrates the effect of a decrease in the rate constants of reactions involving ion formation and sequestration of H_2SO_3 in simulations of the bromate-sulfite reaction. This plot is produced by including reaction 10 in the model with k_{10} s^{-1} = $10/\omega_0^2$ and setting all forward rate constants in the model to $k' = k\omega_0^2/200$.

The Unstirred System: Reaction Fronts. A reaction front is defined as a propagating interface converting reactants to products. In autocatalytic solution-phase systems, the front travels with constant speed that depends on the diffusion coefficient of the autocatalyst, D, and some characteristic reaction time scale, τ:[47]

$$c \approx \sqrt{D/\tau} \tag{11}$$

In general, diffusion coefficients depend on particle size r and dynamic viscosity η of the medium through the Stokes−Einstein equation

$$D = \frac{k_B T}{6\pi\eta r} \tag{12}$$

where k_B = boltzmann's constant, and T = temperature. The reaction time scale in the bromate-sulfite reaction depends on the rate-determining steps of buffer removal (reaction 1) and autocatalysis (reaction 4). Fronts in the aqueous phase are driven by the diffusion of acid. An additional influence on the speed of the bromate-sulfite fronts is reaction-induced convection. The reaction is exothermic but the isothermal density difference between products and reactants is positive. The front propagation is sensitive to double-diffusive convective effects.[48,49] Wave speed is enhanced due to convective fluid motion in both horizontal tubes and ascending or descending fronts in vertical tubes.

Front speeds were obtained in simulations of the bromate-sulfite reaction-diffusion model (eqs 8 and 9 with diffusive terms added) exploiting a 1d domain of spatial step size = 0.001 cm and total length = 1 cm. For the first 3 grid points, $[H^+]$ was set to 1×10^{-4} M to initiate the front. In the aqueous phase, $D = 2 \times 10^{-5}$ cm^2 s^{-1} for small ions. The diffusion coefficient of acid is generally greater than that of the other species in solution; we take $D_H = 4 \times 10^{-5}$ cm^2 s^{-1}. In simulations, the front speed increases from 4−8 mm min^{-1} upon increasing $[BrO_3^-]_{0,aq}$ from 0.05 to 0.1 M (Figure 7d, (i)).

The reaction-diffusion model of the bromate-sulfite reaction may be used to simulate fronts in the w/o microemulsion, assuming that the reaction takes place in the aqueous pseudo phase as described in the previous sections, and the autocatalytic "particle" is now the reverse micelle containing acid. Thus, propagation of the front is driven by diffusion and subsequent collision of the reacted reverse micelles with exchange of their acid contents. With $\omega_0 = 21$ in the TX system, the autocatalytic rate is increased by a factor of 2 (shorter clock time) but the front speed is reduced compared to the aqueous phase by a factor of 9 from 3.6 to 0.4 mm min^{-1}. The reduced front speed is obtained in simulations with $D_H = D = 2.4 \times 10^{-7}$ cm^2 s^{-1} that is, D_H is reduced by a factor of 170 compared to the diffusion coefficient of acid in the aqueous phase (Figure 7d, (ii)). This value compares well with the diffusion coefficients of nanodroplets in a TX w/o microemulsion, which are of the order of 10^{-7}−10^{-6} cm^2 s^{-1}.[24,42]

The decrease in the front speed with increasing ω_0 might be explained by the reduction in the autocatalytic rate (longer clock time) and decrease in the diffusion coefficients of the larger droplets in the more viscous medium as ω_0 increases. In Figure 7e, the values of the front speed close to those observed experimentally were obtained in simulations of the model decreasing the diffusion coefficient from 7×10^{-7} to 7×10^{-8} cm^2 s^{-1}.

The clock time is slightly shorter than in the aqueous phase with $\omega_0 = 12.5$ in the CTAB w/o microemulsion, and the front speed is reduced by a factor of 9. In a CTAB w/o microemulsion, diffusion coefficients of reverse micelles are reported to be of the order of 10^{-7}−10^{-6} cm^2 s^{-1}.[50] The experimentally observed front speed is obtained in simulations by a reduction in D_H of the order of a factor of 130 to 3×10^{-7} cm^2 s^{-1}.

In tubes of diameter 1 mm, there is no trend in front speed with increasing ω_0 in the CTAB w/o microemulsion. The autocatalytic rate increases by a factor of 3 when the value of ω_0 is doubled so for no trend to be observed in front speed, the change in reaction time scale and diffusion coefficients with ω_0 must oppose each other. With the assumption that there is an increase in the average size of the nanodroplets with increasing ω_0, there will be a decrease in the diffusion coefficient of the reverse micelles. The experimental trend is obtained in simulations by increasing the diffusion coefficient from $D = 3 \times 10^{-7}$ to 2×10^{-6} cm^2 s^{-1} (Figure 7e).

However, it is unlikely that the diffusion coefficient of the reverse micelles decreases by a factor of 10 upon doubling the value of ω_0 in this system because the viscosity of the medium decreases while the conductivity remains roughly constant, and the water fraction is only increased by 5%. The reaction-diffusion model may not be appropriate as the fronts may be subjected to convective effects that are more pronounced at lower ω_0. Indeed, in larger tubes (i.d = 2.6 mm) we observe an increase in wave speed with decreasing ω_0 and the formation of convective fingers at the interface between the reacted and unreacted fluid (Figure 6). The structures observed in this system more resemble those of flame fronts, suggesting that the mobility of the reacted fluid, in particular the viscosity, differs greatly from that of the unreacted. Such structures are not observed in the aqueous phase. In 1 mm tubes, the profile of the front is much more diffuse in the CTAB system than in the aqueous phase fronts. This is also indicative of convective effects possibly driven by changes in viscosity upon reaction. Terms involving convective transport may be required to simulate front propagation even in tubes of 1 mm i.d.. This will be the subject of further investigation.

Conclusions

The acid autocatalytic bromate-sulfite reaction is demonstrated to be sensitive to the microenvironment, in particular

the molar ratio of water to surfactant, ω_0, when performed in a w/o microemulsion. Clock times increase with increasing ω_0 in a TX (neutral) w/o microemulsion and decrease with increasing ω_0 in a CTAB (cationic) w/o microemulsion. The overall pH change decreases with ω_0 in the TX system while the initial and final pH is shifted to higher values in the CTAB system. The influence of the w/o microemulsion on the characteristics of the clock reaction is explained by assuming the reactants are trapped in nanosized water droplets, the size of which increase with increasing ω_0. Exact determination of rate constants of processes in the hydrated reverse micelle is difficult due to the heterogeneity of the microenvironment. However, these experiments allow us to determine, in a general sense, the effect of the composition of the w/o microemulsion on the reaction time scale.

We have demonstrated that the w/o microemulsions support propagating acid reaction fronts, the characteristics of which depend on the composition of the medium. Simulations of the bromate-sulfite reaction were performed to illustrate the possible effects of changing ω_0 on the clock kinetics and front speeds. For the latter, we considered the system as an aqueous pseudophase with front propagation driven by diffusion of the reverse micelles containing the autocatalyst, but further investigation is required to determine whether this is an appropriate model.

Acknowledgment. The authors thank the EPSRC for funding.

References and Notes

(1) Luisi, P. L.; Giomini, M.; Pileni, M. P.; Robinson, B. H. *Biochim. Biophys. Acta* **1988**, *947*, 209.
(2) Pileni, M. P. *Nat. Mater.* **2003**, *2*, 145.
(3) Holmberg, K. *Eur. J. Org. Chem.* **2007**, 731.
(4) Lopez-Quintela, M. A.; Tojo, C.; Blanco, M. C.; Rio, L. G.; Leis, J. R. *Curr. Opin. Colloid Interface Sci.* **2004**, *9*, 264.
(5) Fendler, J. H. *Acc. Chem. Res.* **1976**, *9*, 153.
(6) Bru, R.; Sanchezferrer, A.; Garciacarmona, F. *Biochem. J.* **1995**, *310*, 721.
(7) Bagchi, B. *Chem. Rev.* **2005**, *105*, 3197.
(8) Bhattacharyya, K.; Bagchi, B. *J. Phys. Chem. A* **2000**, *104*, 10603.
(9) Ekwall, P.; Mandell, L.; Fontell, K. *J. Colloid Interface Sci.* **1970**, *33*, 215.
(10) Bhattacharyya, K. *Acc. Chem. Res.* **2003**, *36*, 95.
(11) Kwon, O. H.; Kim, T. G.; Lee, Y. S.; Jang, D. J. *J. Phys. Chem. B* **2006**, *110*, 11997.
(12) Vanag, V. K.; Boulanov, D. V. *J. Phys. Chem.* **1994**, *98*, 1449.
(13) Baruah, B.; Roden, J. M.; Sedgwick, M.; Correa, N. M.; Crans, D. C.; Levinger, N. E. *J. Am. Chem. Soc.* **2006**, *128*, 12758.
(14) Vanag, V. K.; Epstein, I. R. *Phys. Rev. Lett.* **2001**, *8722*.
(15) Vanag, V. K.; Epstein, I. R. *Science* **2001**, *294*, 835.
(16) Pojman, J. A.; Ilyashenko, V. M.; Khan, A. M. *J. Chem. Soc., Faraday Trans.* **1996**, *92*, 2825.
(17) Sivashinsky, G. I. *Ann. Rev. Fluid Mech.* **1983**, *15*, 179.
(18) Jaffe, L. F. *Proc. Natl. Acad. Sci. U.S.A.* **1991**, *88*, 9883.
(19) Xin, J. *SIAM Rev.* **2000**, *42*, 161.
(20) De Wit, A. *Phys. Rev. Lett.* **2001**, *8705*.
(21) Edblom, E. C.; Luo, Y.; Orban, M.; Kustin, K.; Epstein, I. R. *J. Phys. Chem.* **1989**, *93*, 2722.
(22) Szanto, T. G.; Rabai, G. *J. Phys. Chem. A* **2005**, *109*, 5398.
(23) Pojman, J. A.; Epstein, I. R. *J. Phys. Chem.* **1990**, *94*, 4966.
(24) Almgren, M.; Vanstam, J.; Swarup, S.; Lofroth, J. E. *Langmuir* **1986**, *2*, 432.
(25) Ekwall, P.; Mandell, L.; Solyom, P. *J. Colloid Interface Sci.* **1971**, *35*, 266.
(26) Vanag, V. K.; Melikhov, D. P. *J. Phys. Chem.* **1995**, *99*, 17372.
(27) Menger, F. M.; Yamada, K. *J. Am. Chem. Soc.* **1979**, *101*, 6731.
(28) Vanag, V. K.; Hanazaki, I. *J. Phys. Chem.* **1996**, *100*, 10609.
(29) Moulik, S. P.; Paul, B. K. *Adv. Colloid Interface Sci.* **1998**, *78*, 99.
(30) Barzykin, A. V.; Tachiya, M. *J. Phys. Chem.* **1994**, *98*, 2677.
(31) Infelta, P. P.; Gratzel, M.; Thomas, J. K. *J. Phys. Chem.* **1974**, *78*, 190.
(32) Williamson, F. S.; King, E. L. *J. Am. Chem. Soc.* **1957**, *79*, 5397.
(33) Hanazaki, I.; Rabai, G. *J. Chem. Phys.* **1996**, *105*, 9912.
(34) Zagora, J.; Voslar, M.; Schreiberova, L.; Schreiber, I. *Phys. Chem. Chem. Phys.* **2002**, *4*, 1284.
(35) Zagora, J.; Voslar, M.; Schreiberova, L.; Schreiber, I. *Faraday Discuss.* **2001**, *120*, 313.
(36) Rabai, G.; Kaminaga, A.; Hanazaki, I. *J. Phys. Chem.* **1996**, *100*, 16441.
(37) Andrade, S. M.; Costa, S. M. B. *Photochem. Photobiol. Sci.* **2002**, *1*, 500.
(38) Pant, D.; Levinger, N. E. *Langmuir* **2000**, *16*, 10123.
(39) Andrade, S. M.; Costa, S. M. B.; Pansu, R. *J. Colloid Interface Sci.* **2000**, *226*, 260.
(40) Rodriguez, R.; Vargas, S.; Fernandez-Velasco, D. A. *J. Colloid Interface Sci.* **1998**, *197*, 21.
(41) Gu, J. Y.; Schelly, Z. A. *Langmuir* **1997**, *13*, 4256.
(42) Mo, C. S. X. *Langmuir* **2002**, *18*, 4047.
(43) Zhu, D. M.; Wu, X.; Schelly, Z. A. *J. Phys. Chem.* **1992**, *96*, 7121.
(44) Rodenas, E.; Valiente, M. *Colloid Surf.* **1992**, *62*, 289.
(45) Fang, X. L.; Yang, C. F. *J. Colloid Interface Sci.* **1999**, *212*, 242.
(46) Faeder, J.; Ladanyi, B. M. *J. Phys. Chem. B* **2005**, *109*, 6732.
(47) Luther, R. *Z. Elektrochem. Z.* **1906**, *12*, 596.
(48) Keresztessy, A.; Nagy, I. P.; Bazsa, G.; Pojman, J. A. *J. Phys. Chem.* **1995**, *99*, 5379.
(49) Nagy, I. P.; Keresztessy, A.; Pojman, J. A. *J. Phys. Chem.* **1995**, *99*, 5385.
(50) Giustini, M.; Palazzo, G.; Colafemmina, G.; DellaMonica, M.; Giomini, M.; Ceglie, A. *J. Phys. Chem.* **1996**, *100*, 3190.